Aerodynamic angle estimation: comparison between numerical results and operative environment data

CEAS Aeronautical Journal manuscript No.
(will be inserted by the editor)

Aerodynamic Angle Estimation: Comparison Between Numerical Results and Operative Environment Data

Angelo Lerro · Manuela Battipede · Piero Gili · Alberto Brandl

Received: date / Accepted: date

Abstract Several architectures exist to measure aerodynamic angles based on physical sensors. As far as Unmanned Aerial Vehicle (UAV) is concerned, traditional systems hardly comply with reliability and redundancy requirements due to size and weight limitations. A patented virtual sensor, based on Artificial Neural Network (ANN) techniques, named Smart-Air Data, Attitude and Heading Reference System (Smart-ADAHRS) has been investigated as a good estimator for aerodynamic angles in simulated environment. This paper focuses on flight testing procedures in operative environment and data processing for the Smart-ADAHRS validation with real data. As many factors interfere during the generation of the ANN training set, an accurate choice and integration of the Flight Test Instrumentation (FTI) system components becomes crucial. A comprehensive description has been included about the FTI equipment and its influence on the neural network performance. Differences between numerical simulation and operative environment data are detailed as final aim of this work. At the end, feasible solutions are suggested to solve the typical gap between virtual and real scenario, both in terms of data analysis and neural network architecture.

Keywords Aerodynamic angles · Flight test · Neural network · Operative environment comparison · Virtual sensor

Angelo Lerro, E-mail: angelo.lerro@polito.it
Manuela Battipede, E-mail: manuela.battipede@polito.it
Piero Gili, E-mail: piero.gili@polito.it
Alberto Brandl, E-mail: alberto.brandl@polito.it
Department of Mechanical and Aerospace Engineering (DIMEAS)
Politecnico di Torino, corso Duca degli Abruzzi, 24 - Turin (ITALY)

Glossary

ADAHRS Air Data, Attitude and Heading Reference System
ADS Air Data System
ADU Air Data Unit
ANN Artificial Neural Network
AOA Angle of Attack
AOS Angle of Sideslip
FCS Flight Control System
FEK FTE Electronic Kneepad
FTE Flight Test Engineer
FTI Flight Test Instrumentation
GA General Aviation
MLP Multilayer Perceptron
NSSE Normalized Sum-of-Squares Error
PDF Probability Density Function
SFDIA Sensor Fault Detection, Isolation and Accommodation
Smart-ADAHRS Smart-Air Data, Attitude and Heading Reference System
SHSS Steady Heading Sideslip
TRL Technology Readiness Level
UAV Unmanned Aerial Vehicle
ULM Ultra Light Machine

Symbols

n_i acceleration as measured by an accelerometer on ith axis
q pitch rate
q_c impact pressure
r yaw rate
α Angle of Attack
β Angle of Sideslip

θ pitch angle
ϕ roll angle
i_{Body} ith Body axis
$\hat{x}$ Initial estimation of the signal x
$\dot{x}$ Time derivative of the signal x

1 Introduction

The continuous challenge of the aeronautical research is mainly related to performance improvement and environmental impact reduction of the aircraft and its related products. Despite a great extent of research has been promoted in avionics, aircraft instrument technology for aerodynamic angle measurement has not seen significant innovation since the first half of the XX century. When developing a new aircraft avionic product, the main challenges are related to low cost, high reliability, small size, low weight and eco-friendly features. These requirements are harder to meet when considering an Unmanned Aerial Vehicle (UAV). Generally speaking, design requirements for small and medium UAV limit available space and maximum take-off weight to strict values (see [12]). Moreover, many electronic sensors and hardware components are needed in order to enable remote piloting. In order to ensure reliability for UAV systems, aircraft equipment is frequently duplicated or triplicated in a typical hardware redundancy. This is in conflict with the previous described design approach. For these reasons, software solutions have been developed, such as analytical redundancy, with the aim to integrate virtual sensors in modern avionics that introduce the chance to simulate a generic system without adding any physical component [40]. One of the most common aircraft system is the Air Data System (ADS) which is highly demanding in terms of space, weight and costs. Common ADSs are made up of several probes, transducers and Air Data Unit (ADU) and provide the pilot (or the Flight Control System (FCS), especially in case of unmanned aircraft) with a complete air dataset including all information about aerodynamic interaction between the aircraft and the external flow.

Different ADS sensor configuration exist with the aim to be compliant with specific requirements related to particular applications ranging from the General Aviation (GA) to the military aircraft (see [34] [6] [3] [2] [1] [4] [5] [7]). However, ADS systems always rely on external sensors. This introduces some issues related to position errors, installation, de-icing systems, power requirements and maintenance tasks. Recently, literature has intensively investigated the field of Sensor Fault Detection, Isolation and Accommodation (SFDIA) [27] [32] [33] and some papers exist proposing solutions which tackle ADS sensor faults [48] [39]. However, to the best of our knowledge, the Technology Readiness Level (TRL) of those solutions remained low. Moreover, this paper addresses a method which aims to reduce the total number of external sensors, instead of accommodating their faults. A patented technology, based on soft computing techniques, named Smart-Air Data, Attitude and Heading Reference System (Smart-ADAHRS) [35] have demonstrated to be an accurate and reliable replacement for complex and expensive traditional ADS (see [18], [16], [17] [20], [21]). The Smart-ADAHRS technology enables to reduce external ADS devices (sensors and probes) and simplifies the entire ADS architecture taking advantage of an innovative sensor fusion algorithm, different from the classical Kalman Filter [25] [24]. In fact, only one external source of dynamic and static pressure is required. Previous research addressed to validate the algorithm in simulated environment, considering sensor noise and atmospheric turbulence [18]. Different architectures have been studied, with different input vectors. This paper will focus on the Artificial Neural Network (ANN) without surface control signal in the input vector, which is considered an important simplification [37] that brings significant advantages for common ADS [36]. The smart solution proposed here applies an Multilayer Perceptron (MLP) to fill the gap between an initial estimator and the actual value of the target signal [17]. This methodology can virtually obtain a good accuracy on aerodynamic angle values, suitable for typical aircraft control systems. After being fully validated in a simulated environment, both in clean and turbulent atmosphere on the De Havilland DHC-2 Beaver mathematical model [44], the sensor has been tested on an actual ultralight aircraft. This paper focuses on the comparison between simulated values and real operative environment data obtained during relevant flight tests. As the recorded values are used both for training and test the ANN, additional care must be taken during the design of the Flight Test Instrumentation (FTI) system since it highly influences the learning process. In fact, errors on data calibration and signal synchronization, as well as data logger faults or poor FTI sensor performance, could affect the ANN training. Moreover, mechanical behaviour of external probes (such as natural frequency) might influence the learning phase. Therefore, an accurate analysis of data logs cannot take place without a suitable FTI platform.

This paper begins with a general introduction of the MLP training and of the signal reconstruction procedure itself. A comprehensive description of the FTI equipment and of the way it affects the output performance is included in Section 3. Section 3 shows also the statistical features selected in order to analyse the final

results showed in Section 4. Differences between numerical simulations and operative environment results are detailed as the main aim of this work. At the end, feasible solutions are suggested to solve the typical gap between virtual and real scenario, both in terms of data analysis and MLP architecture.

2 Neural Network for Air Data Estimation

As generally known, aerodynamic forces and moments acting on aircraft are function of interactions between the body and the external flow [14] [26]. This, indeed, influences vehicle dynamics itself and justifies the importance of the determination of what are called Air Data. Monitoring this dataset is fundamental and some fatal accidents occurred in the past due to malfunctioning of the ADS [9] [11]. ADS is then considered a safety-critical aircraft system, currently made of several external sensors (see [36]). This paper deals with the estimation of the relative angles between the aircraft Body reference frame and the Air Trajectory frame, the so-called aerodynamic angles: Angle of Attack (AOA) (or α) and Angle of Sideslip (AOS) (or β). However, this operation is here performed with virtual sensors. During the last decades, virtual sensors demonstrated to be cost effective techniques in several areas [41] and some research projects were focused on AOA as well. For instance, a proposed virtual sensor for the AOA estimation [40] that splits in three parts the signal to recompose: a trimmed angle of attack obtained by means of a Takagi-Sugeno fuzzy model, a short period AOA obtained from linear short period approximation and a third part calculated by a neural network. In [28] the estimation of Calibrated Air Speed (CAS) and AOA are obtained by means of an Adaptive Kalman Filter (AEKF). The same paper proposes an approach based on the aerodynamic model inversion (AMI), as described in [29]. Among the model-learned solutions, [42] proposes a method where the identification of the aerodynamic coefficient, from sparse data, has been conducted using ANN trained as described in [43]. A different algorithm is described in [47], where a Functional Pooling Nonlinear AutoRegressive with eXogenous excitation (FP-NARX) is applied in order to directly obtain the AOA signal.

This paper deals with a very straightforward model, suitable for real-time and cost effective innovative avionic systems. Consider the following linearization of α and β:

$$\alpha = \hat{\alpha} + \Delta\alpha \tag{1}$$

$$\beta = \hat{\beta} + \Delta\beta \tag{2}$$

where $\hat{\alpha}$ and $\hat{\beta}$ are linear estimation obtained with flight mechanics equations whereas $\Delta\alpha$ and $\Delta\beta$ are the differences between the linear estimations and the true nonlinear angles. According to a patented procedure ([35]), the initial estimation of the angle of attack $\hat{\alpha}$ and sideslip angle $\hat{\beta}$ is augmented with the evaluation of $\Delta\alpha$ and $\Delta\beta$ based on two MLPs, which process measurements obtained with non-protruding sensors (except for the Pitot tube).

$\hat{\alpha}$ and $\hat{\beta}$ can be evaluated as follows:

$$\hat{\alpha} = \theta - \gamma \tag{3}$$

$$\hat{\beta} = K\frac{n_y}{q_c} \tag{4}$$

where θ stands for the pitch angle, γ for the flight path angle, n_y is the acceleration measured by the accelerometer along the Y_{Body} axis and q_c is the impact pressure. K allows to adjust the measure units and typically has a value between $20\,\mathrm{kg\,m^{-2}}$ and $40\,\mathrm{kg\,m^{-2}}$.

An MLP is made up of several layers. Each layer consists of a set of nonlinear squashing functions (meaning functions bounded by their horizontal upper and lower asymptotes) evaluated on a linear composition of the preceding output values. This function composition allows to represent any map under some assumptions and this property makes the MLP a universal approximator. During the training phase, the weights of the MLP are tuned in order to fit the data selected for training. At the end, a function is obtained and it can be validated and tested with a second set of data. This process is similar to apply the linear regression on a set of values. The difference is that the linear regression will always find a straight line (in the 2D case) fitting the data, whereas the MLP does not have a fixed model. Actually, the model itself depends on the weights. A huge amount of literature exists about the MLP as performing as a universal approximator. Refer to [19] [22] [15] [23] [31] [30] for the relevant mathematical demonstration. During the training procedure, the weights of the linear combinations are estimated solving the nonconvex problem of the error function optimization. Different heuristic rules exist and the most common is the Levenberg-Marquardt (LM) algorithm. However, this application deals with a big amount of data, making the employment of the LM rule not feasible. The training rule applied in this article is the Resilient Propagation (RPROP). The complete input vector needed by Smart-ADAHRS includes data from the GPS, the ADS and the AHRS (Attitude and Heading Reference System) which provide body accelerations, angular rates and attitude, as can be seen in Fig. 1. The Pitot-tube is the only external source of data.

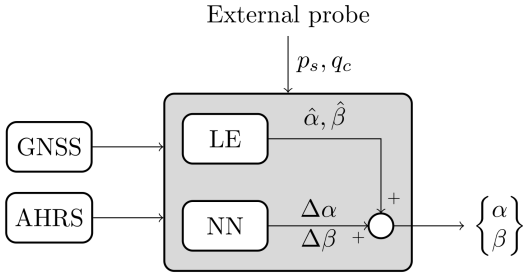

Fig. 1 General schematic of the Smart-ADAHRS

Actually, an intrinsic redundancy seems to exist among the set of measurements. Previous research showed that analytic evaluation is indeed feasible for the evaluation of α and β, thanks to this apparent redundancy. Analysis of the influence of the input vector on results allowed the reduction of the total number of signals effectively needed by the network. At first, control system signals where applied as input to the MLPs but in some cases they could be unavailable, as in small UAV, Ultra Light Machines (ULMs) or GA aircraft. The following feed-forward predictors are hence implemented:

$$\Delta\alpha = f_\alpha \left(q_c, \dot{q}_c, n_x, n_z, \theta, q, \hat{\alpha}\right) \tag{5}$$

$$\Delta\beta = f_\beta \left(q_c, \dot{q}_c, n_x, n_y, n_z, \phi, r, \hat{\beta}\right) \tag{6}$$

where q_c is the impact pressure, $\dot{q}_c$ is the time derivative of q_c, n_x, n_y, n_z are the accelerations measured by the accelerometers respectively on X_{Body}, Y_{Body} and Z_{Body} axes, ϕ is the roll angle, r is the yaw rate, θ the pitch angle, q is the pitch rate and $\hat{\alpha}$ and $\hat{\beta}$ are the initial linear estimation for the angle of attack and the sideslip angle respectively. Previous research activities on simulated turbulent environment in [18] showed the possibility of considering previous time steps of the input vector in a Time Delay Network. This practice however is not here implemented because, at this phase, it was preferred to start with a simpler model. Furthermore, the computational cost would increase and the system would require a memory buffer big enough to manage an augmented input vector. The main aspect of considering the turbulent environment is the necessity of training the neural network using noisy signals which are representative of the stochasticity of turbulence. An error, calculated as the difference between the estimated angle and the real angle, is here considered acceptable if it is bounded between $\pm 2^\circ$ and if it holds this value for at least 10 s. Obviously, the only information about the error bounds is not enough because the harmonic content of the residuals is also of great interest for such applications. For sake of clarity, a constant error, periodic oscillations or white noise acting on the signal will have different consequences. However, the error analysis will show a mean error very close to 0°, so the bounds will indeed apply only to the dynamical behaviour of the residuals.

3 Methodology

Previous sections are focused on the advantages of implementing an MLP in an ADS. Moreover, the mathematical background needed to fully understand how this algorithm works has been depicted. This section starts with the description of how training and test sets have been collected in both simulated and real environment. The second part deals with the selection of suitable parameters to conduct a proper comparison between simulations and flight testing. An ideal solution to perform a comparison between real and simulated scenarios would need the implementation of the same aircraft model on a flight simulator, undergoing to exactly the same input signals. Unfortunately, this is not possible at this stage. Firstly, a detailed aerodynamic and dynamic identification of the test aircraft was not available at the time of writing this article. The Ultra Light Machine (ULM) applied for the flight test campaign is currently under development and still some modifications on the design can occur. Secondly, the flight tests have a parallel final aim of demonstrating aircraft compliance with the current technical airworthiness regulations. Moreover, what a real test pilot can actually lead is limited by the practical feasibility of the manoeuvres themselves. On the other hand, during simulations, the aircraft can be virtually placed in some conditions that a real pilot would not reach for security reasons. It must be noted that it is not easy to obtain a time history which can describe the entire flight envelope of the aircraft. For these reasons, a simultaneous training with several recorded manoeuvres has been carried out, as described in [36]. As mentioned above, a set of trajectories have been obtained by means of a flight simulator of the DHC-2 Beaver aircraft based on the FDC toolbox [44]. Time histories of the command signals and trim conditions have been defined on the basis of the experience gained during previous research. Another set of trajectories have been obtained by means of a flight test campaign, where an ULM has been equipped with a complete FTI system. This data collection is the result of a collaboration between different entities. A prototype of the Smart-ADAHRS, currently able to record all the input signals needed by the MLP, has been developed by Politecnico di Torino and AeroSmart srl. Target values (AOA and AOS) are measured by the FTI developed by the Politecnico di Milano, which manages the flight test campaign of the

Table 1 Neural Network description

Hyperparameter	Value
Architecture	MLP
Number of MLPs	2 (1 x AOA, 1 x AOS)
Number of hidden layers	1
Number of neurons per each layer	13
Activation function	Sigmoid function
Input size (AOA Network)	7
Input size (AOS Network)	8
Training set size (simulation)	$\sim$ 660k entries
Training set size (flight test)	$\sim$ 510k entries
Heuristic rule	RPROP
Max number of iterations	1000
# of training repetitions	10
Training data partitioning	YES
% of data used to update gradients	70 %
% of data used for test	15 %
% of data used for validation	15 %

ULM. The test aircraft is manufactured by Ing. Nando Groppo srl and is called G-70. After the selection of suitable training time histories, data have been pre-processed to span the set $[-1; 1]$. This is because the Universal Approximation Theorem states that an MLP is able to uniformly approximate any function inside the $[0; 1]^n$ hypercube. Please note the numerical differences between the two lower bounds is not really an issue, because the input layer weights will easily scale the input range. The important fact is that the input space is lower-and-upper-bounded. Before testing the ANN, the procedure verifies that the manoeuvre is a subset of the training set, for at least the major part. After the pre-processing of the training and test sets, a single layer MLP with 13 neurons is trained with simulated data and compared to another MLP trained with flight test data. This procedure is repeated twice, the first one to estimate $\Delta\alpha$ and the second one on $\Delta\beta$. Briefly, each function in Eq. 6 is modeled by an MLP. Training is repeated 10 times to avoid local minima and the network with the minimum validation error is considered the best solution. The heuristic rule applied for training is the RPROP. Table 1 shows the main hyperparameters of the MLPs.

3.1 Flight Test Instrumentation

The ultralight aircraft has been equipped with a complete FTI to record all signals necessary to the Smart-ADAHRS. As mentioned above, the test equipment can be divided in two main groups. The first one, called Mnemosine, is a complete FTI developed by Politecnico di Milano, able to record all inertial and air data from various sensors. It features a low cost, reliable, flexible and low intrusive solution for flight testing operation and it has been tailored for ULM. The fifth version of this equipment is composed by a Mnemosine Main Unit (MMU) that groups the main nodes of the system as the GPS unit, a card manager to store data and the galvanically-isolated electrical power supply for the entire FTI, with the possibility of using an auxiliary external battery for the on-ground operations. Air Data Unit has been maintained independent to keep the installation close to the two air data booms, mounted under the wings. The right half-wing air data-boom was equipped with two vanes, respectively for AOA and AOS, whereas the left one featured a total pressure probe. Signals coming from these probes have been transduced and recorded by an ADS, composed by a micro-controller board Olimex STM32-5107 and a signal conditioning module. Moreover, Mnemosine provides a WiFi Telemetry Unit complying the 802.11n wireless protocol, using two omnidirectional antennae, mounted on the lower aft part of the fuselage. The Flight Test Engineer (FTE) is equipped with the FTE Electronic Kneepad (FEK) that allows him/her to mark relevant events of the test flights. Refer to [45] for additional information. The second group of the test equipment is related to the prototype, subject of this article. It is composed by a very high accuracy AHRS named Spatial, integrated with an ADU, both by Advanced Navigation (see [10] and [13]). According to the standard, the AHRS is composed by an inertial and a GPS unit integrated with a Kalman-like filter. The output of the ADAHRS is recorded by the Smart-ADAHRS prototype. The latter is currently composed by two programmable boards able to record the signals in input. Table 2 lists the equipment used during flight tests.

Table 2 FTI description

System	Model (Producer)	Role
ADAHRS	Spatial (Advanced Navigation)	Main
ADS	Air Data Boom (Aerosonic Corp.)	Main
AHRS	MTi (Xsens)	Redundancy
GPS	LEA-6R (ublox)	Redundancy
FTI Manager	Mnemosine	Main

In this investigation, several effects can influence the accuracy of the measurements. For example, the reciprocating engine can generate a spectrum of oscillations on the metallic structure of the aircraft. Moreover, atmospheric turbulence can affect the Pitot-booms, although tests are not performed in heavy turbulent air. Structural vibrations can affect both inertial sensors and the aerodynamic fins. The propeller wake itself induces velocity on the Pitot-booms. At the same time,

Table 3 Sampling frequency

System	Sampling frequency
Primary ADS	10 Hz
Secondary GPS	2 Hz
Secondary AHRS	50 Hz

each sensor has its own nonlinearities, affecting the quality of the recorded signals. Background noises and dynamic response of each sensor must be taken into account when the experiment is set up. For these reasons, the signals obtained from flight tests can be much noisier than those coming from simulated environment. However, a good training will avoid the data over-fit, allowing the ANN to learn only the underlined model.

3.2 Data synchronization

A preliminary data analysis induced the authors to consider the heterogeneity of the sampling frequency of the different systems (Table 3).

Moreover, due to hardware delay, the sampling frequency of the primary ADAHRS is not constant. Accurate data pre-processing is hence required to get a unique time base, over which re-interpolate every signal. In this work, the final sampling frequency has been set to 100 Hz. This operation has been performed by means of a properly written MATLAB® routine.

3.3 Comparison Analysis

As indicated above, a method to compare the results obtained by Smart-ADAHRS is needed. The selected parameters should give an indication which is independent from the input trajectory or the aircraft model. For this reason, the comparison of the time histories is based on the classical descriptive statistical features, as upper bound and lower bound, mean error and standard deviation (see [46]). Additionally, a graphical comparison of the error distribution before and after the application of the nonlinear estimator has been carried out. Moreover, it must be remembered that in case of real flight test measurements, the sensor signal is strongly affected by the external noise. In order to have an estimation of the signal stability, each signal has been processed with a 20-th order median filter. The standard deviation of the residuals between the filtered signals and the actual ones has been computed and compared among the various cases. For similar applications, for example the analysis of the bias stability in MEMS sensors, the Allan deviation is often computed [8]. However, it must be noted that the information coming from the computation of the Allan deviation are influenced by the general trend of the signal. In fact, the Allan deviation is usually evaluated on the basis of a null input recording, to study the sensor background noise. In this case, structural vibrations, the contingent aircraft dynamics and disturbances related to the sensor installation affect the sensor signals in several ways during the trajectory. The analysis of the still sensors would not detect the various effects, obtaining a non comprehensive estimation. These techniques should show the improvements given by the application of the algorithm with respect to linear estimation.

4 Results

This section shows the input and output statistical features, comparing the measurements obtained from simulations with those recorded during flight test campaigns.

4.1 Training and test set

The training set should cover the widest portion of flight envelope. Several flight manoeuvres were conducted by a certified pilot on the same aircraft during a flight test campaign, which was protracted for several months. The entire set of recorded flight tests should have generated a comprehensive list of manoeuvre, suitable for the construction of the training and test pattern for the ANN. After the flight campaign has been completed, suitable time windows of the recorded data have been selected. Situations with flap conditions different from 0° have been avoided, because flaps definitely change the aircraft configurations and training could be degraded. This could be seen as a limitation of the current analysis. However, the approach is actually applicable to every condition. If additional data is available in flaps down condition, the MLP will obtain good results even in this configuration. Further investigations will be conducted to verify this aspect.

Table 4 Training manoeuvres, flight test

Maneuvers	Total time [s]
Sawtooth glides, Dutch Roll	2320
Sawtooth glides, Dutch Roll	1970
Phugoid (stick fixed and stick free)	420
Steady Heading Sideslip	480

A brief description of the training and test trajectories applied for the real scenario is resumed in Table 4 and Table 5. This selection has been obtained with

a trial and error procedure. It should be noticed that including a manoeuvre strictly related to the lateral-directional plane as could be the Steady Heading Sideslip (SHSS) can improve the final test results. This could be due to the various flight conditions that are encountered in a real scenario, hardly limited only to the longitudinal plane. Fig. 2 shows the AOA-AOS envelope of the training and test set in operative environment. A primary zone and an extended zone have been highlighted, where the Smart-ADAHRS must ensure a certain level of uncertainty.

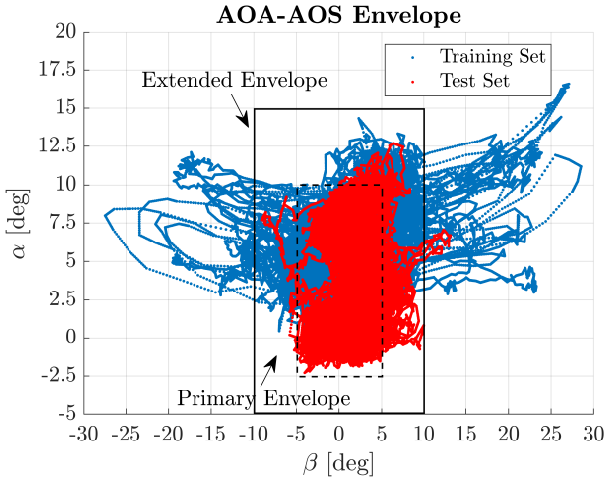

Fig. 2 AOA-AOS Envelope for the operative environment training and test set

After data have been synchronized and prepared to be applied to the ANN, initial promising results have been obtained. The error trend is a good symptom for the training and test operations conducted with data coming from the operative environment. In fact the error, though not entirely bounded into $\pm 2°$, exceeds these values for a limited amount of time.

Table 5 Test manoeuvres, flight test

Maneuvers	**Total time** [s]
Sawtooth glides	580
Sawtooth glides, Phugoid (stick fixed and stick free)	1900
Sawtooth glides	900

For the simulated environment, a set of manoeuvres have been properly defined. As previously discussed, the comparison between real and simulated scenario has not been conducted on the same aircraft for the same trajectories. Hence, this set of sample manoeuvres has been selected to meet two different goals: the first one is to have a good description of the aircraft dynamics, in order to obtain a good training set; the latter is to have some sort of similarities with the flight test time histories. Table 6 provides a description of the simulated manoeuvres. Fig. 3 shows the AOA-AOS envelope of the training and test set in simulated environment.

Table 6 Simulated manoeuvres

Maneuvers	**Total time** [s]
Pitch angle steps	2200
Pitch angle steps (different trim conditions)	2200
Roll angle steps	2200
Yaw angle steps	2200
Mixed pitch and roll angle steps	2200
Sawtooth glides	1660
Stall	1630
Trim	2200
Mixed maneuver	1070

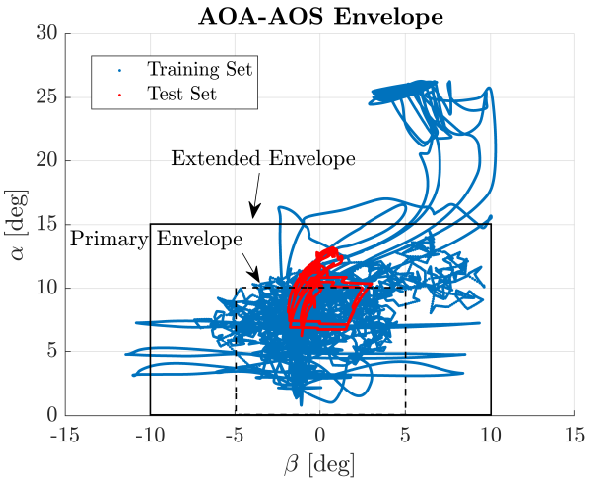

Fig. 3 AOA-AOS Envelope for the simulated environment training and test set

An example of the sawtooth glide manoeuvres in the simulated environment can be seen in Fig. 4. The corresponding flown trajectory is in Fig. 5. In Fig. 6 can be seen an example of a SHSS performed during flight test.

A graphical interpretation of the ability of a training manoeuvre to cover the flight envelope can be conducted with the box and whiskers plots [38]. The normalized input signals used for training in the simulated scenario can be seen in Fig. 7 and Fig. 8, whereas the corresponding analysis for the real scenario can be seen in Fig. 9 and Fig. 10. Middle lines represent the medians and the boxes delimit the regions between the 25th and 75th quartiles. Whiskers extend for 1.5 times the difference between the 75th and 25th quartiles before

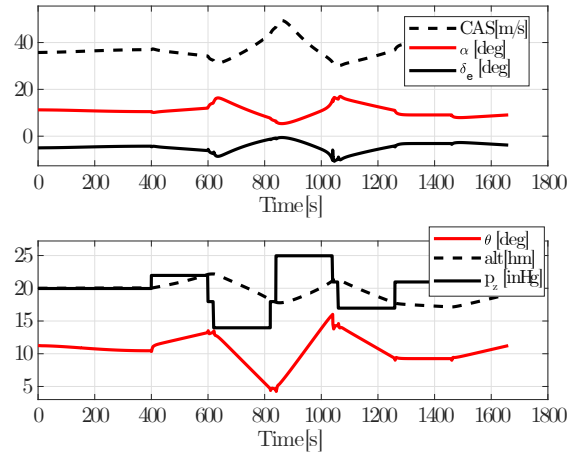

Fig. 4 Details of simulated sawtooth glides

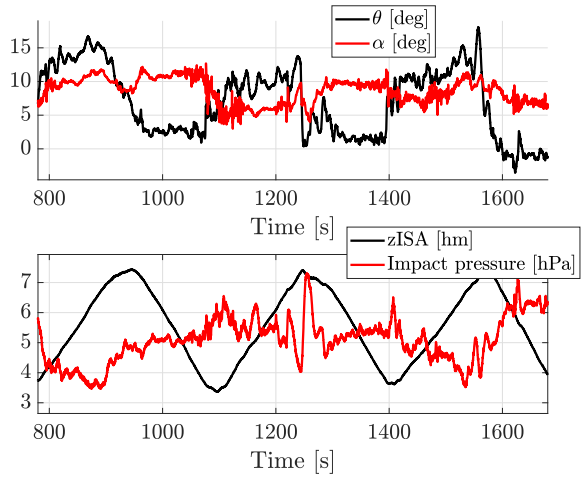

Fig. 5 Details of sawtooth glides conducted on 10th June

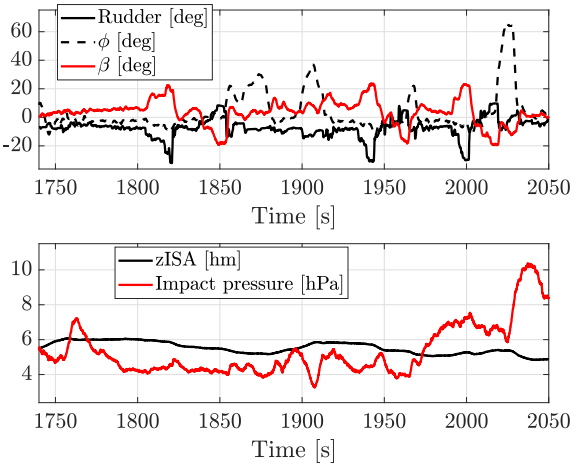

Fig. 6 Details of SHSS conducted on 10th June

and after the 25th and 75th quartiles themselves. Other data are considered outliers and are individually plotted with a red plus sign. As can be seen from Fig. 7 to Fig. 10, a large part of the training set is composed by outliers. In those regions, the training performance will be degraded, which implies that a thicker coverage on training is recommended.

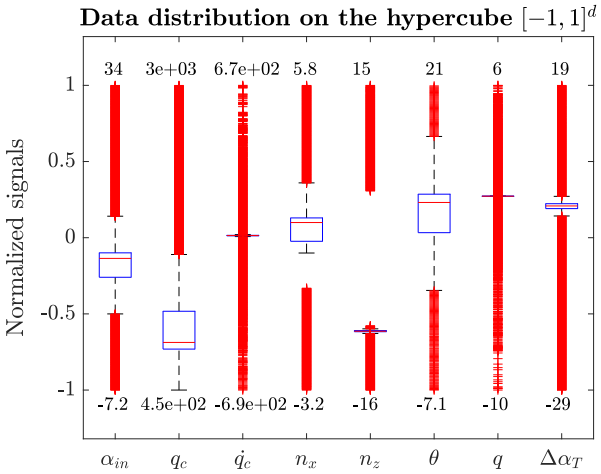

Fig. 7 Graphical visualization of the normalized input range for training (simulation, AOA target). Minimum and maximum values are reported. Units are as follows: angles in °, pressure in Pa, accelerations in $\mathrm{m\,s^{-2}}$, angular rates in $\mathrm{rad\,s^{-1}}$

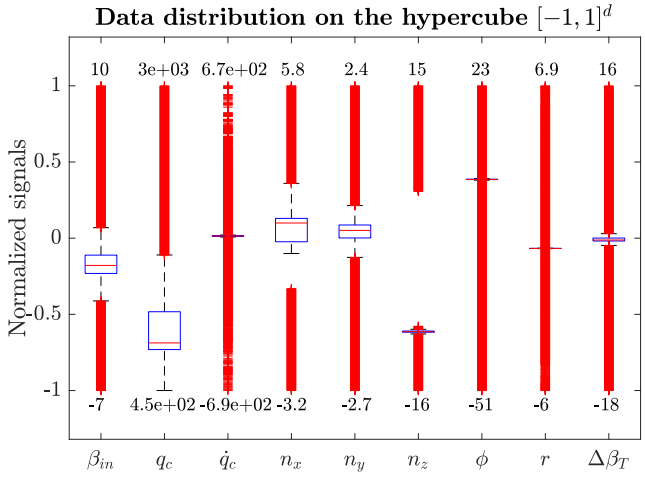

Fig. 8 Graphical visualization of the normalized input range for training (simulation, AOS target). Minimum and maximum values are reported. Units are as follows: angles in °, pressure in Pa, accelerations in $\mathrm{m\,s^{-2}}$, angular rates in $\mathrm{rad\,s^{-1}}$

A comparison of the standard deviation of the differences between the actual and the filtered signals can be performed analysing Fig. 11 and Fig. 12. Results are

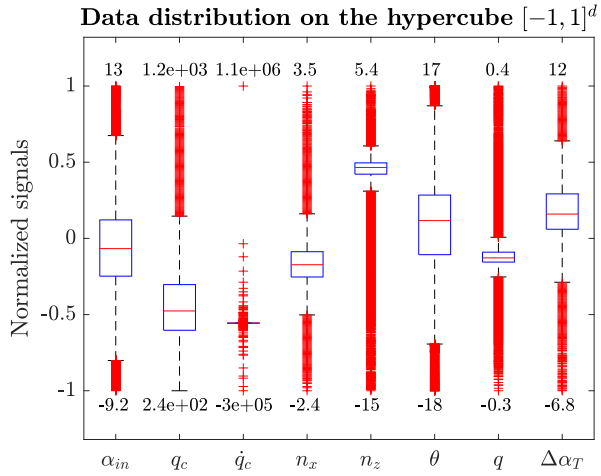

Fig. 9 Graphical visualization of the normalized input range for training (flight test, AOA target). Minimum and maximum values are reported. Units are as follows: angles in °, pressure in Pa, accelerations in $\mathrm{m\,s^{-2}}$, angular rates in $\mathrm{rad\,s^{-1}}$

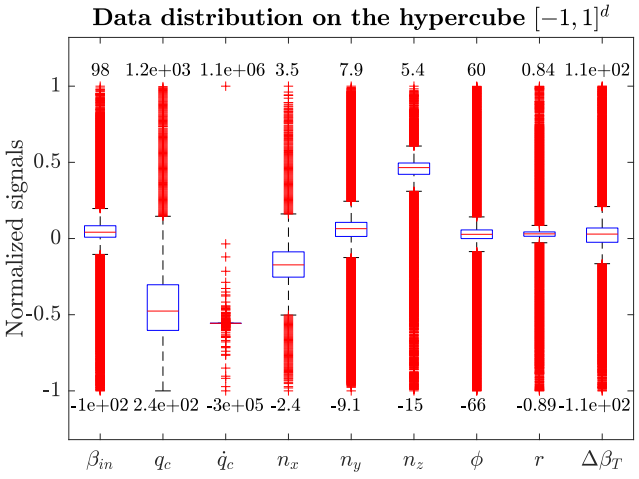

Fig. 10 Graphical visualization of the normalized input range for training (flight test, AOS target). Minimum and maximum values are reported. Units are as follows: angles in °, pressure in Pa, accelerations in $\mathrm{m\,s^{-2}}$, angular rates in $\mathrm{rad\,s^{-1}}$

similar for the AOS network and they have not been reported here. It should be noticed that they represent the signals already mapped into the $[-1;1]^n$ hypercube. Flight test data has only one order of magnitude higher values, maybe due to the low order of the median filter, together with the scaling effect of the pre-processing.

As far as test data are concerned, only some appreciable results are reported. Fig. 13 shows the box and whiskers plot for the third test trajectory in the simulated environment, corresponding to an elevator step in a trim condition which differs from the training set. The entire manoeuvre is clearly a subset of the training set. Moreover, the residual standard deviations shown

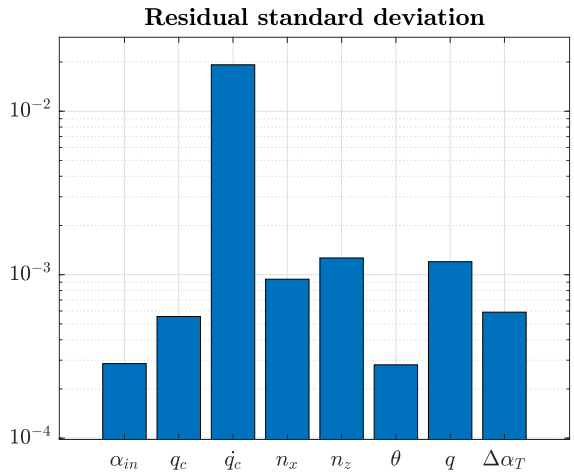

Fig. 11 Residual standard deviation of the training set (simulation, AOA target, nondimensional values)

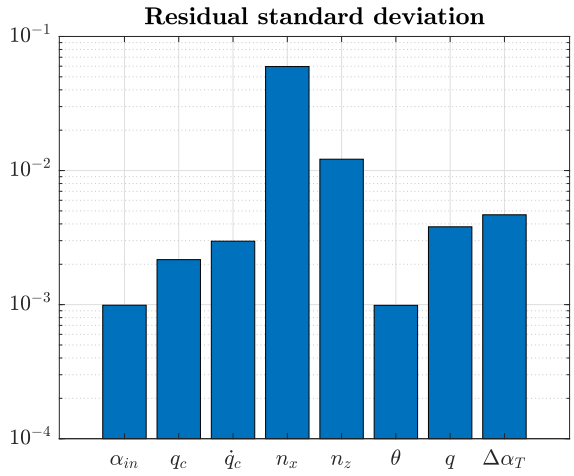

Fig. 12 Residual standard deviation of the training set (flight test, AOA target, nondimensional values)

in Fig. 15 are very low, compared to those obtained during training.

In operative environment, residual standard deviations are of the same order of magnitude of the training set as can be seen in Fig. 16. At the same time, the shown manoeuvre is not completely contained in the training trajectories, as can be seen in Fig. 14, where the normalized impact pressure distribution contains values greater than 1.

4.2 Smart-ADAHRS performance

Four MLPs (two for AOA estimation and two for AOS estimation) have been trained with trajectories containing stalls, sawtooth glides and aileron input steps; its performance have been evaluated in different manoeu-

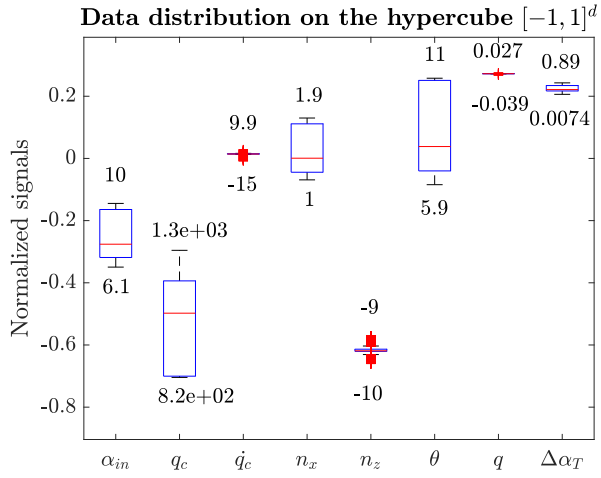

Fig. 13 Graphical visualization of the normalized input range for test, trajectory #3 (simulation). Minimum and maximum values are reported. Units are as follows: angles in °, pressure in Pa, accelerations in $\mathrm{m\,s^{-2}}$, angular rates in $\mathrm{rad\,s^{-1}}$

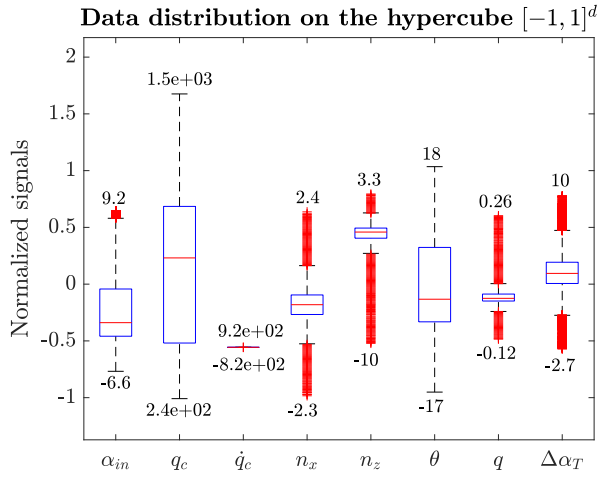

Fig. 14 Graphical visualization of the normalized input range for test, trajectory #2 (flight test). Minimum and maximum values are reported. Units are as follows: angles in °, pressure in Pa, accelerations in $\mathrm{m\,s^{-2}}$, angular rates in $\mathrm{rad\,s^{-1}}$

vres, in order to study their generalization capabilities. Training performance are shown in Fig. 17 and Fig. 18. The observed behaviour is quite different. Despite the order of magnitude of the Normalized Sum-of-Squares Error (NSSE) is almost the same, in the simulated environment the training operation spreads over solutions with different final NSSE.

Using flight test data, the trend is smoother among the 10 training operations. This could be due to the noise and signal disturbances, which act on the weight tuning as a leveller of the error function local minima. Fig. 19 and Fig. 21 show a comparison between the target AOA, the linear estimation and the output of

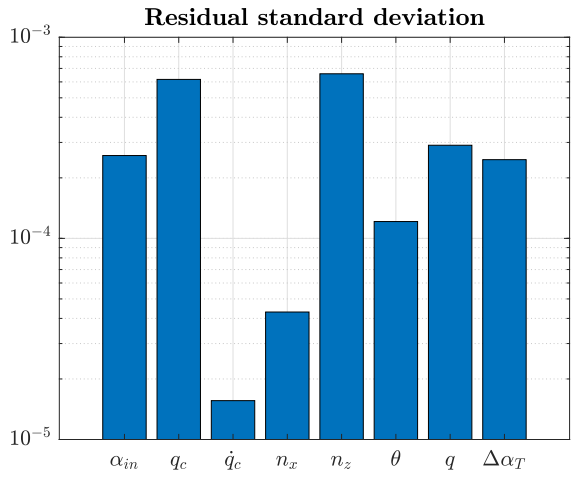

Fig. 15 Residual standard deviation of the trajectory #3 of the simulated test set (AOA target, nondimensional values)

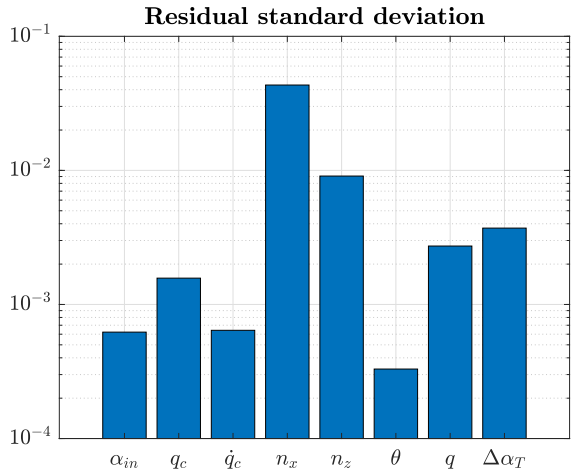

Fig. 16 Residual standard deviation of the trajectory #2 of the flight test set (AOA target, nondimensional values)

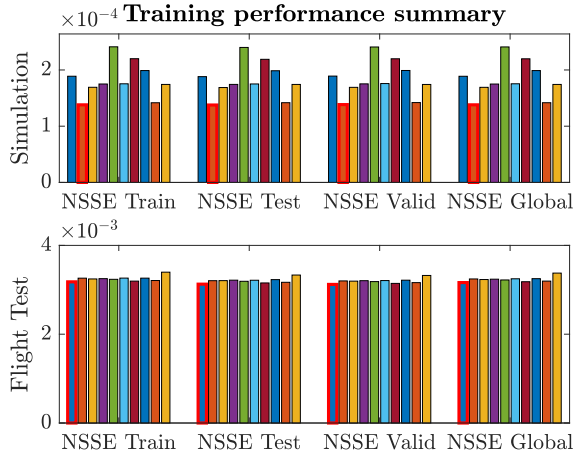

Fig. 17 Training performance in terms of NSSE for AOA estimation

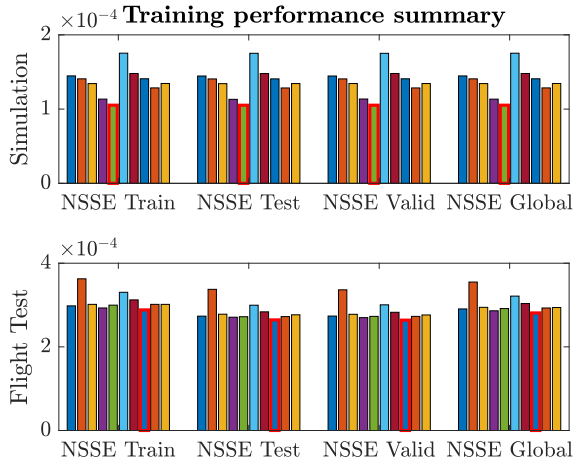

Fig. 18 Training performance in terms of NSSE for AOS estimation

the Smart-ADAHRS. As it can be seen, in the simulated environment the estimation error is smoother than in the flight test case and bounded between $-0.6°$ and $0.6°$.

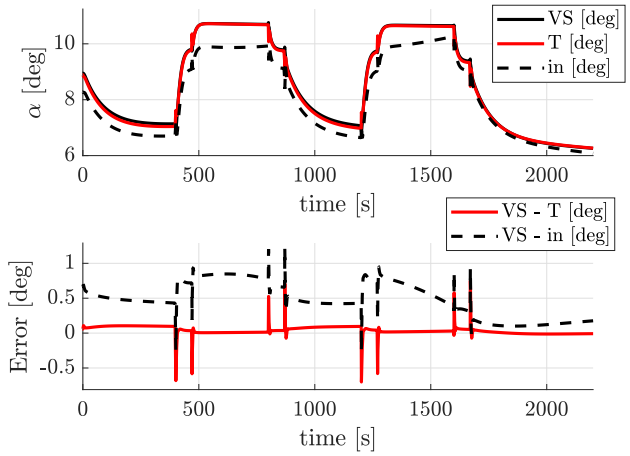

Fig. 19 Output comparison between true angle (α_T), linear estimation (α_{in}) and the output of the virtual sensor (α_{VS}) for trajectory #3 of the simulated test set

The improvements on the AOA evaluation between the initial estimation and the Smart-ADAHRS estimation for the simulated environment can be seen in Fig. 23. Fig. 24 shows the error PDF in case of operative environment. In this latter case, the effect of the MLP is clear. In fact, the asymmetric error distributions becomes 0-mean and almost symmetric after the estimation of $\Delta\alpha$.

The same comparison can be done on the AOS estimation. Fig. 20 and Fig. 22 show an example of test

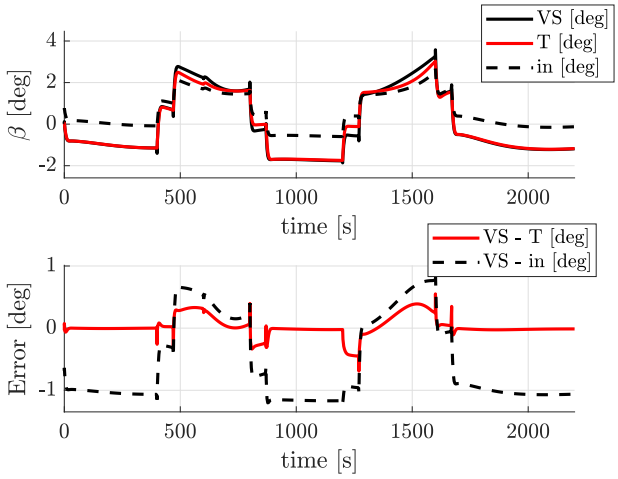

Fig. 20 Output comparison between true angle (β_T), linear estimation (β_{in}) and the output of the virtual sensor (β_{VS}) for trajectory #4 of the simulated test set

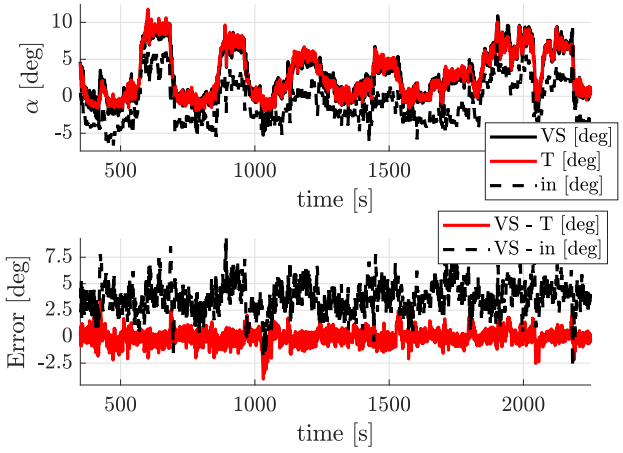

Fig. 21 Output comparison between true angle (α_T), linear estimation (α_{in}) and the output of the virtual sensor (α_{VS}) for trajectory #2 of the flight test set

trajectory respectively for the simulated and operative environment. In this case, the estimation uncertainty is wider than in case of AOA estimation. This is mainly due to the fact that the flight envelope should be better covered among the different values of β. Future flight test campaigns will be conducted in order to face this problem. Fig. 25 and Fig. 26 allow to compare the error PDF between simulated and operative environment.

These promising results show the confirmed reduction of the estimation error between the linear and the nonlinear model. These figures provide the evidence that the algorithm can work well also in operative environment, where several external disturbances exist on the input signals. A comparison on the output performance between simulated and real environments shows

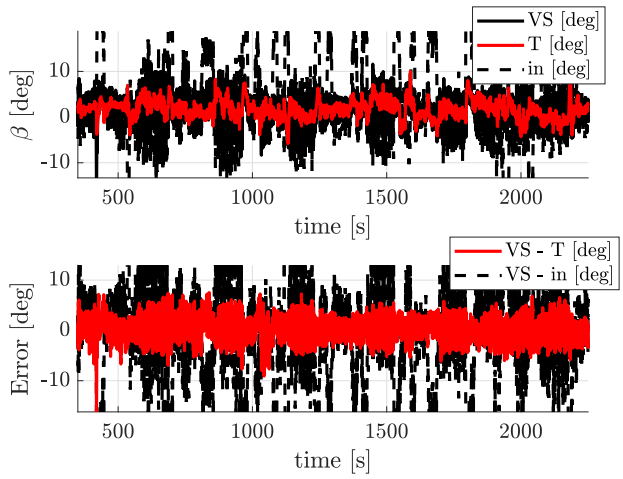

Fig. 22 Output comparison between true angle (β_t), linear estimation (β_{in}) and the output of the virtual sensor (β_{VS}) for trajectory #2 of the flight test set

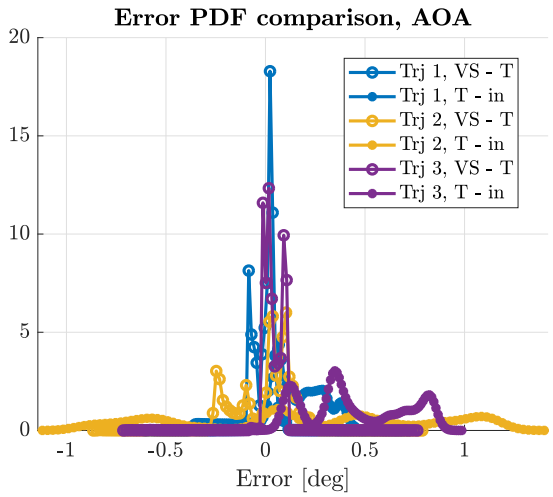

Fig. 23 Error PDF for trajectory #1 , #2 and #3 of the simulated test set (Target: AOA)

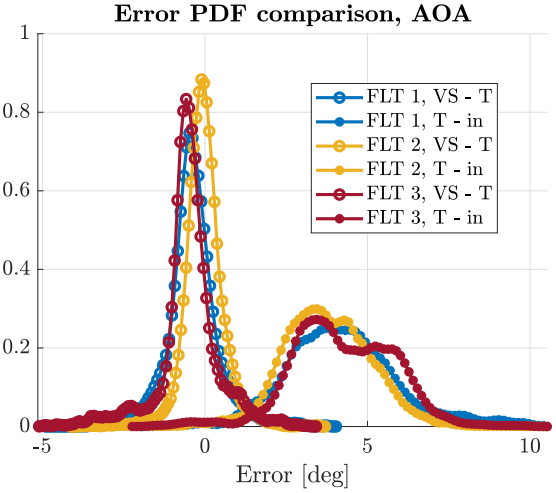

Fig. 24 Error PDF for trajectory #1 , #2 and #3 of the flight test set (Target: AOA)

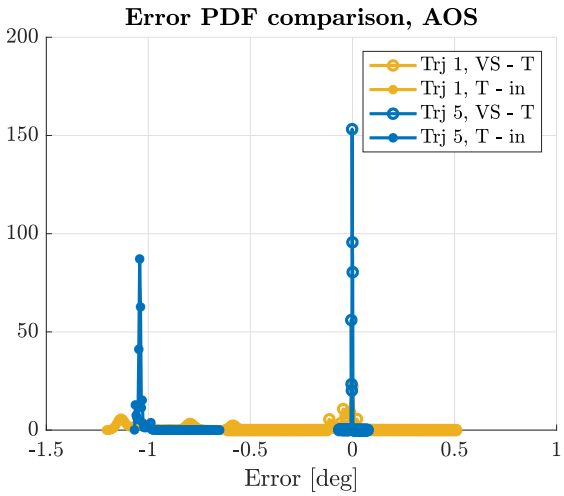

Fig. 25 Error PDF for trajectory #1 and #5 of the simulated test set (Target: AOS)

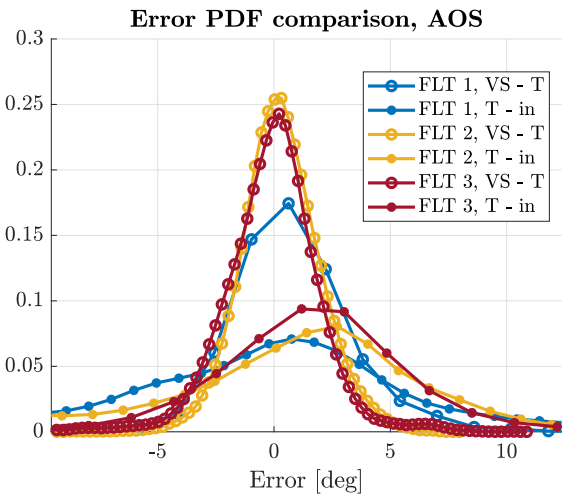

Fig. 26 Error PDF for trajectory #1 , #2 and #3 of the flight test set (Target: AOS)

an evident increase of the final error range. However, it should be noticed that the upper and lower bounds are subject only to a slight increase. Moreover, the reduction of the mean error found in the simulated environment is confirmed also in the real scenario. Although the FTI equipment has been conceived under the requirements of reducing the external sensitivities, a residual error on the target signal is still detectable. This obviously affects the training procedure and hence the ability of the nonlinear estimator to reduce the estimation error. Table 7 and Table 8 report mean values and standard deviations of the residual errors before and after the application of the MLP. The mean error value has always been reduced, in some cases even dropped by two orders of magnitude. Only in one case the error standard deviation has been increased. How-

ever, this might be considered an outlier and a different training set might be useful to avoid this situation.

5 Conclusions

The estimation of Air Data without using external sensors is a good challenge for tomorrow aircraft. At the same time, aerodynamic angles are fundamental signals for what concerns the control of the aircraft. This paper shows how Smart-ADAHRS can be applied to operative environment data with good accuracy and how the input pattern should be built in order to obtain good results. After the general description of the ANN, the FTI equipment had been described, focusing on main threats that can influence the measurements. Analysis of the input data and output performance have been carried out studying the main statistical features of the signals. Four versions of the Smart-ADAHRS have been obtained training two MLPs respectively with simulated and flight test data, both for the AOA and AOS. A good similarity has been obtained between the two cases, confirming the initial supposition. The behaviour during training has been discussed and test performance have been analysed. The showed results provide compelling evidence that the underlined model can be learned and the approach can be effective in the reduction of the estimation error.

Acknowledgements The authors would like to thank Ing. Nando Groppo srl and Politecnico di Milano for their collaboration and support during the flight test campaign.

References

1. Aircraft sensors and systems total air probe. Tech. rep., AMETEK Aerospace. Wilmington, USA
2. Angle of attack transducer. Tech. rep., AMETEK Aerospace. Wilmington, USA
3. Sensors. Tech. rep., Aerosonic Corporation. Clearwater, USA
4. State-of-the-art air data products solution guide. Tech. rep., SpaceAge Control. Palmdale, USA
5. Magnetic angle of attack sensor. Tech. rep. (2001). WO 01/77622 A2
6. Angle of attack (aoa) sensors. Tech. rep., UTC Aerospace Systems (2005). Burnsville, USA
7. Multi-function air data sensing probe having an angle of attack vane. Tech. rep. (2005). US 6941805 B2
8. IEEE Standard Specification Format Guide and Test Procedure for Single-Axis Interferometric Fiber Optic Gyros (2008)
9. Easa airworthiness directive ad no.: 2013-0068. Tech. rep., EASA (2013). 29 March
10. Air data unit reference manual. Tech. rep., Advanced Navigation (2015)
11. Easa airworthiness directive ad no.: 2015-0135. Tech. rep., EASA (2015). 15 July
12. Mezzi aerei a pilotaggio remoto. Tech. rep., ENAC (2015). July, 2nd ed
13. Spatial reference manual. Tech. rep., Advanced Navigation (2015)
14. Anderson Jr, J.D.: Fundamentals of aerodynamics. Tata McGraw-Hill Education (2010)
15. Attali, J.G., Pagès, G.: Approximations of functions by a multilayer perceptron: a new approach. Neural Networks **10**(6), 1069–1081 (1997). DOI 10.1016/S0893-6080(97)00010-5. URL http://linkinghub.elsevier.com/retrieve/pii/S0893608097000105
16. Battipede, M., Cassaro, M., Gili, P., Lerro, A.: Novel Neural Architecture for Air Data Angle Estimation, pp. 313–322. Springer Berlin Heidelberg, Berlin, Heidelberg (2013). DOI 10.1007/978-3-642-41013-0_32. URL http://dx.doi.org/10.1007/978-3-642-41013-0_32
17. Battipede, M., Gili, P., Lerro, A.: Neural Networks for Air Data Estimation: Test of Neural Network Simulating Real Flight Instruments, pp. 282–294. Springer Berlin Heidelberg, Berlin, Heidelberg (2012). DOI 10.1007/978-3-642-32909-8_29. URL http://dx.doi.org/10.1007/978-3-642-32909-8_29
18. Battipede, M., Gili, P., Lerro, A., Caselle, S., Gianardi, P.: Development of neural networks for air data estimation: Training of neural network using noise-corrupted data. In: 3rd CEAS Air & Space Conference, 21st AIDAA Congress, pp. 1–10 (2011)
19. Bishop, C.M.: Neural Networks for Pattern Recognition. Clarendon Press Oxford (1995)
20. Brandl, A., Battipede, M., Gili, P., Lerro, A.: Sensitivity analysis of a neural network based avionic system by simulated fault and noise injection. In: 2018 AIAA Modeling and Simulation Technologies Conference. American Institute of Aeronautics and Astronautics (2018). DOI doi:10.2514/6.2018-0122. URL https://doi.org/10.2514/6.2018-0122
21. Brandl, A., Lerro, A., Battipede, M., Gili, P.: Air data virtual sensor: a data-driven approach to identify flight test data suitable for the learning process. In: 5th CEAS Conference on Guidance, Navigation and Control, pp. 1–16 (2019)
22. Castro, J., Mantas, C., Benítez, J.: Neural networks with a continuous squashing function in the output are universal approximators. Neural Networks **13**(6), 561–563 (2000). DOI 10.1016/S0893-6080(00)00031-9. URL http://linkinghub.elsevier.com/retrieve/pii/S0893608000000319
23. Cybenko, G.: Approximation by superpositions of a sigmoidal function. Mathematics of Control, Signals and Systems **2**(4), 303–314 (1989). DOI 10.1007/BF02551274. URL https://doi.org/10.1007/BF02551274
24. De Vivo, F., Battipede, M., Gili, P., Brandl, A.: Ill-conditioned problems improvement adapting joseph covariance formula to non-linear bayesian filters. In: W. Press (ed.) WSEAS Transactions on Electronics, vol. 7, p. 1825 (2016). DOI 10.13140/RG.2.1.3027.0960
25. De Vivo, F., Brandl, A., Battipede, M., Gili, P.: Joseph covariance formula adaptation to square-root sigma-point kalman filters. Nonlinear Dynamics **88**(3), 1969–1986 (2017). DOI 10.1007/s11071-017-3356-x. URL https://doi.org/10.1007/s11071-017-3356-x
26. Etkin, B., Reid, L.D.: Dynamics of flight. Wiley New York (1971)
27. Gertler, J.J.: Survey of model-based failure detection and isolation in complex plants. IEEE Control Systems Magazine **8**(6), 3–11 (1988). DOI 10.1109/37.9163

Table 7 Test manoeuvres, mean error results

Environment	Trajectory	Mean error True - Linear [°]		Mean error Virtual Sensor - True[°]	
		AOA	AOS	AOA	AOS
Sim	1	0.1268	-0.9331	-0.0044	-0.0330
Sim	2	0.2071	-0.8240	-0.0030	0.0149
Sim	3	0.4435	-0.8020	0.0391	-0.1682
Sim	4	-0.0361	-0.5745	0.0276	0.0243
Sim	5	0.0275	-1.0388	0.0268	-0.0015
Flt	1	4.2770	-3.3235	-0.3879	0.7247
Flt	2	3.7613	-1.0050	-0.0388	0.2761
Flt	3	4.2463	-0.9885	-0.4966	-0.1284

Table 8 Test manoeuvres, standard deviation results

Environment	Trajectory	1σ error True - Linear [°]		1σ error Virtual Sensor - True[°]	
		AOA	AOS	AOA	AOS
Sim	1	0.1734	0.1948	0.0596	0.0501
Sim	2	0.6234	0.2260	0.1414	0.0537
Sim	3	0.2473	0.0909	0.0632	0.1431
Sim	4	0.3037	0.5785	0.0491	0.1576
Sim	5	0.0189	0.0222	0.0034	0.0043
Flt	1	1.8123	10.7858	0.8115	2.6464
Flt	2	1.3338	11.3806	0.6077	1.7575
Flt	3	1.5561	13.8051	0.9182	2.1956

28. Hardier, G., Seren, C., Ezerzere, P.: Modelbased techniques for virtual sensing of longitudinal flight parameters. International Journal of Applied Mathematics and Computer Science **25**(1), 23–38 (2015). DOI 10.1515/amcs-2015-0002. URL http://content.sciendo.com/view/journals/amcs/25/1/article-p23.xml
29. Hardier, G., Seren, C., Ezerzere, P., Puyou, G.: Aerodynamic model inversion for virtual sensing of longitudinal flight parameters. In: 2013 Conference on Control and Fault-Tolerant Systems (SysTol), pp. 140–145. IEEE (2013). DOI 10.1109/SysTol.2013.6693835. URL http://ieeexplore.ieee.org/document/6693835/
30. Haykin, S.: Neural networks: a comprehensive foundation. Prentice Hall PTR (1994)
31. Hornik, K.: Approximation capabilities of multilayer feedforward networks. Neural Networks **4**(2), 251 – 257 (1991). DOI https://doi.org/10.1016/0893-6080(91)90009-T. URL http://www.sciencedirect.com/science/article/pii/089360809190009T
32. Isermann, R.: Model-based fault-detection and diagnosis - Status and applications. Annual Reviews in Control **29**(1), 71–85 (2005). DOI 10.1016/j.arcontrol.2004.12.002. URL http://www.sciencedirect.com/science/article/pii/S1367578805000052
33. Isermann, R., Ballé, P.: Trends in the application of model-based fault detection and diagnosis of technical processes. Control Engineering Practice **5**(5), 709 – 719 (1997). DOI https://doi.org/10.1016/S0967-0661(97)00053-1. URL http://www.sciencedirect.com/science/article/pii/S0967066197000531
34. Lenschow, D.H.: Vanes for sensing incidence angles of the air from an aircraft. Journal of Applied Meteorology **10**(6), 1339–1343 (1971). DOI 10.1175/1520-0450(1971)010⟨1339:VFSIAO⟩2.0.CO;2. URL http://journals.ametsoc.org/doi/abs/10.1175/1520-0450{\%}281971{\%}29010{\%}3C1339{\%}3AVFSIAO{\%}3E2.0.CO{\%}3B2
35. Lerro, A., Battipede, M., Gili, P.: System and process for measuring and evaluating air and inertial data (2013). Patent No. EP3022565A2
36. Lerro, A., Battipede, M., Gili, P., Brandl, A.: Advantages of neural network based air data estimation for unmanned aerial vehicles. International Journal of Mechanical, Aerospace, Industrial, Mechatronic and Manufacturing Engineering **11**(5), 1016 – 1025 (2017). URL http://waset.org/Publications?p=125
37. Lerro, A., Battipede, M., Gili, P., Brandl, A.: Survey on a neural network for non linear estimation of aerodynamic angles. In: Proceedings of the 2017 Intelligent Systems conference (IntelliSys), vol. 1, pp. 929–935. IEEE (2017)
38. McGill, R., Tukey, J.W., Larsen, W.A.: Variations of box plots. The American Statistician **32**(1), 12–16 (1978)
39. Oliveira, J.C.M., Pontes, K.V., Sartori, I., Embiruçu, M.: Fault detection and diagnosis in dynamic systems using weightless neural networks. Expert Systems with Applications **84**(Supplement C), 200 – 219 (2017). DOI https://doi.org/10.1016/j.eswa.2017.05.020. URL http://www.sciencedirect.com/science/article/pii/S0957417417303366
40. Oosterom, M., Babuska, R.: Virtual sensor for the angle-of-attack signal in small commercial aircraft. In: 2006 IEEE International Conference on Fuzzy Systems, pp. 1396–1403. IEEE (2006). DOI 10.1109/FUZZY.2006.1681892. URL http://ieeexplore.ieee.org/document/1681892/
41. Palma, G., Scognamiglio, O., Lavorgna, M.: Low cost virtual pressure sensor. In: SAE Technical Paper, pp. 1–15. SAE International (2004). DOI 10.4271/2004-01-1367. URL http://dx.doi.org/10.4271/2004-01-1367
42. Rajkumar, T., Bardina, J.: Prediction of aerodynamic coefficients using neural networks for sparse data. In: FLAIRS, pp. 242–246 (2002)
43. Rajkumar, T., Bardina, J.: Training data requirement for a neural network to predict aerodynamic coefficients. p. 92 (2003). DOI 10.1117/12.

486343. URL http://proceedings.spiedigitallibrary.org/proceeding.aspx?doi=10.1117/12.486343
44. Rauw, M.: Fdc 1.2 - a simulink toolbox for flight dynamics and control analysis. Tech. rep. (2001)
45. Rolando, A., Rossi, F., Castelletti, T., Reghenzani, F.: Mnemosine Mark-V: The Fifth Generation of an Ultra Light Machine-Dedicated FTI System. In: 27th Annual Society of Flight Test Engineers European Chapter Symposium, pp. 1–12 (2016)
46. Ross, S.M.: Introduction to probability and statistics for engineers and scientists. Academic Press (2014)
47. Samara, P.A., Fouskitakis, G.N., Sakellariou, J.S., Fassois, S.D.: Aircraft angle-of-attack virtual sensor design via a functional pooling narx methodology. In: 2003 European Control Conference (ECC), pp. 1816–1821. IEEE (2003). DOI 10.23919/ECC.2003.7085229. URL https://ieeexplore.ieee.org/document/7085229/
48. Samy, I., Gu, D.W.: Lecture Notes in Control and Information Sciences. Springer-Verlag Berlin Heidelberg (2011). DOI 10.1007/978-3-642-24052-2